Hydroxyapatite formation on Metallurgical Grade Nanoporous Silicon Particles

E.G. Chadwick [1, 3], O.M. Clarkin [1, 2] and D.A. Tanner [1, 3*]

[1]Materials & Surface Science Institute, [2] Clinical Materials Unit, [3] Department of Manufacturing and Operations Engineering, University of Limerick,
Ireland

*E-mail: david.tanner@ul.ie, Tel: 00-353-(0)61-234130; Fax: 00-353-(0)61-202913

Keywords: Porous Silicon (PS); Hydroxyapatite (HA); Simulated Body Fluid (SBF); Bioactive materials; Scanning Electron Microscopy (SEM); Transmission Electron Microscopy (TEM); Energy Dispersive X-ray Spectroscopy (EDX); X-ray Photoelectron Spectroscopy (XPS).

Abstract: Studies into bone-like apatite or hydroxyapatite (HA) growth on potential biomaterials when in contact with simulated body fluid (SBF) not only establish a general method for determining bioactivity but coincidently lead to the design of new bioactive materials in biomedical and tissue engineering fields. Previous studies of HA growth on porous silicon have examined electrochemically etched silicon substrates after immersion in a simulated body fluid. This study differs from previous work in that it focuses on characterising HA growth on chemically etched metallurgical grade nanoporous silicon particles. The porous silicon (PS) used in this study is comprised of nanosponge particles with disordered pore structures with pore sizes ranging up to 10nm on micron sized particles. The silicon particles are analysed before and after immersion into SBF using scanning electron microscopy (SEM), transmission electron microscopy (TEM), energy dispersive x-ray (EDX) analysis and x-ray photoelectron spectroscopy (XPS). Results indicate that a HA layer forms on the surface of the nanosponge particles. Experimental analysis indicates that the morphology and calcium-to-phosphorus ratio (Ca/P) verify the formation of crystalline HA on the nanoporous silicon particles.

1. Introduction

A bioactive material is one that is designed to elicit or modulate biological activity [1]. A prerequisite for a potential bioactive material is the formation or growth of HA on the surface of the material once in contact with body fluids [2]. HA is the basic component of natural bone [3]. It is now accepted that materials capable of forming this bone-like apatite in SBF will likely bond directly to bone upon implantation [4]. It is also considered that an ideal bioactive surface for HA formation might be a porous structured material that would rapidly induce the formation of a physiologically stable HA after immersion into SBF [5]. Porous materials like PS, have received considerable attention from both academia and industry due to their various properties and potential applications in a variety of different fields [6-11].

PS substrates have also been shown to be possible candidate biomaterials following studies establishing their biostability and non-toxicity [5]. The development of micromachining technology has led to PS based devices being used in BIOMEMS and biochip applications [12]. Nanostructured PS is increasingly being used in bio-sensors and drug delivery therapies [7, 13, 14]. In 1995, Canham was the first to explore the idea of PS as a biomaterial with a range of dissolution experiments in SBF [15]. He found that hydrated microporous films of silicon could induce HA growth on themselves and neighbouring areas of bulk silicon and suggested that silicon should be developed as an active biomaterial. PS microparticles have recently been investigated for use in delivering insulin across intestinal tissue and loaded with the isotope ^{32}P to kill tumor cells [16]. The potential applications of PS would now seem abundant. Therefore, it is beneficial to add further knowledge to these fields and investigate the microstructural behaviour and possible bioactivity of chemically etched metallurgical grade nanoporous silicon material as an alternative to the anodised PS materials used by Canham and the majority of other researchers. In this study, standard *in vitro* bioactivity testing is used as described by Kokubo *et al* [4] to determine the possible bioactivity of this material and also establish the basis for future development of new bioactive nanoporous silicon applications.

The Vesta Sciences (North America) process for manufacturing PS consists of using a chemical etching procedure known as stain etching, where metallurgical grade silicon powder is etched in a Hydroflouric acid, Nitric acid and water $HF/HNO_3/H_2O$ solution [10, 17]. This procedure results in a new high surface area material consisting of silicon nanosponge particles with pores disposed throughout each individual particle. This paper outlines work in examining four samples of this silicon powder both before and after immersion in SBF. Examination of the material involves nitrogen adsorption analysis, SEM, TEM, EDX and XPS of the PS particles.

2. Experimental Details

2.1 Porous Silicon Preparation

PS particles were prepared by stain etching bulk metallurgical grade silicon powder from Vesta Ceramics (Sweden) which is sold under the trademark of Sicomill™. The procedure used is a patented etching process carried out by Vesta Sciences [10, 17]. The powders were chemically etched in a nitric acid-hydrofluoric acid mixture as described by Farrell *et al* [17] which induces porosity within the silicon particles. Depending on the orientation of the particles during the etching process not all of the particle surface may be etched - these unetched areas have been observed with high resolution SEM. Some surface areas may contain fewer pores than others. When the etching process is complete, the etched powder is removed from the acid bath and dried in perfluoroalkoxy (PFA) trays at 80°C for 24 hours. By varying the nitric acid concentration in the etchant mixture the surface area of these powders can also be tailored [10, 17]. Four samples of the silicon powder are used in this paper and are described in section 3.1.

2.2 Simulated Body Fluid Trial & Microscopy Analysis

The SBF solution was produced in accordance with the procedure outlined by Kokubo *et al* and cross-referenced with BS ISO 23317:2007 [4, 18]. A JEOL JSM-840 scanning electron microscope equipped with a Princeton Gamma Tech EDX system was used to obtain secondary electron images of the sample surface and EDX spectra were obtained at 20kV, using a beam current of 0.26nA. Quantitative EDX converted the collected spectra into concentration data by using standard reference spectra obtained from pure elements under similar operating parameters. For high resolution SEM analysis the PS samples were spread onto a silver conducting paint on a 15mm aluminum stub and loaded into the Hitachi SU-70 scanning electron microscope. The SEM was operated at 3.0kv with a sample working distance of 3.6mm. TEM specimens were prepared by loading the porous silicon particles onto Formvar-backed carbon-coated copper grids (Agar Scientific, Stanstead, England). TEM analysis was then performed using a JEOL JEM 2100F Field Emission Electron Microscope equipped with an EDX Genesis XM 4 system 60 Energy Dispersive Spectroscopy and operated at 200kV. TEM images were recorded with a Gatan Ultrascan 1000 digital camera. XPS analysis was carried out using a Kratos Axis 165 Spectrometer.

3. Experimental Results and Discussion

3.1 Particle Morphology before immersion in SBF

The Brunauer, Emmett and Teller (BET) [19] surface area and porosimetry analysis was measured by nitrogen gas adsorption in a Micromeritics Gemini V gas adsorption analyzer. The pore size distribution and pore volume were estimated using the Barrett-Joyner-Halenda (BJH) [20] scheme. The results of this analysis are indicated in Table 1. Samples (a) - (d), as listed in Table 1, are nanoporous samples of silicon powder. The average particle size for sample (a) - (c) is about 4-6 microns as determined using SEM measurements. Sample (a) is a 100% chemically etched sample (100% etched is defined as the point when the sample exhibits photoluminescence with an ultraviolet light [17]), with a BET surface area of 103 m^2/g and a pore volume of 0.28 cm^3/g. The average pore size is determined to be approximately 8nm. Sample (b) is a 60% chemically etched sample (the silicon powder sample is etched for 60% of the time), that has the largest pore size of the samples analysed here of 9.6nm. The specific surface area and pore volume is much higher in samples (a) and (c) compared to sample (b). Samples (c) and (d) are 100% chemically etched samples with sample (d) having a much larger average particle size of 20 microns compared to the other samples. The respective surface area, pore volume and pore size was calculated for each sample and tabulated in Table 1.

Table 1 Surface area and porosimetry analysis for the PS samples

	% Etched	BET Surface Area (m^2/g)	Pore Volume (cm^3/g)	Pore Size (nm)
Sample (a)	100%	103	0.28	8
Sample (b)	60%	34	0.11	9.6
Sample (c)	100%	122	0.23*	5
Sample (d)	100%	67	0.11	5

* UL obtained result. Other results were obtained by Vesta Research.

The images in Fig. 1 represent sample (a) and were obtained using high resolution electron microscopy. The inset image in Fig. 1a highlights the centre region around the large pore at high magnification while also showing clearly the dispersion of pores on the surface of the silicon particle. Fig. 1b shows sample (a) analysed using TEM showing the dispersion of pores throughout the particle and the inset image highlights the porosity evident at the outer region of the silicon particle. Electron diffraction studies in TEM indicated that each individual PS particle is a single crystal. Similar results were obtained for all samples analysed in this study.

The particle morphology was studied from a series of SEM images, obtained using the JEOL JSM-840 SEM and a Hitachi SU 70 SEM. Particles were studied at several different magnifications for each sample. The SEM images in Fig. 2 represent samples (a) - (d). Sample (d) clearly shows a larger particle size of about 20 microns compared to an average value of 4-6 microns for samples (a) - (c).

The SEM EDX analysis in Fig. 3 shows the respective EDX spectra for samples (a) and (b) which is also indicative of the results achieved for samples (c) and (d). Apart from the high silicon (Si) peaks, only gold (Au) and Carbon (C) were found present in all the samples. The Au peak is from sputter coating the material prior to SEM analysis. The C peak is from the carbon stub used to mount the PS samples.

XPS was utilised to establish the surface layer composition of the PS particles. The PS samples (a) and (b) showed fluorine, oxygen, carbon and silicon signals as seen in Fig. 4. The respective elemental peaks indicated percentage concentrations of fluorine at 2%, carbon at 28.6%, silicon at 60.2%, and oxygen at 9.2% for sample (a). Sample (b) had slightly less percentage concentrations of fluorine, carbon and oxygen compared to sample (a). Similar results were found for the remaining samples (c) & (d) with those samples having the highest percentage concentrations of oxygen present, as seen in Table 2. Previous studies, where non-oxidized and oxidised PS samples were immersed into SBF proved that PS samples with greater surface levels of oxidation have more regular precipitation of HA than non-oxidized samples [2].

Table 2 XPS % concentrations of surface elements for the PS samples (a)-(d)

% Concentrations	Sample a	Sample b	Sample c	Sample d
Fluorine	2.0	1.3	2.1	1.5
Carbon	28.6	24.5	34.0	28.3
Silicon	60.2	65.6	53.4	57.3
Oxygen	9.2	8.6	10.5	12.8

3.2 Particle Morphology after immersion in SBF

It is an accepted philosophy that materials capable of producing an apatite layer on their surface in SBF may bond directly to bone upon implantation in living bone [21]. The PS samples (a) - (d) were examined after immersion for 30 days in SBF. Bone bonding materials will usually form apatite on their surfaces within four weeks [4]. Thus, a 30 day time period was chosen to allow for the possible development of a thick dense layer of apatite on the nanoporous silicon samples. X-ray diffraction studies were not possible in this case due to sample size available after the SBF trial. TEM nano-beam diffraction was therefore used and is discussed further in section 3.3. In sample (a) (see Fig. 5), it would appear that some of the silicon particles have agglomerated and subsequently an apatite layer coated their surfaces. The development of an apatite layer is again, apparent in sample (c) after 30 days where an apatite layer has formed covering the majority of the silicon particles. The apatite layer is comprised mainly of ball shaped structures which in previous SBF studies have been referred to as apatite granules or spherulites [22]. Results were somewhat similar in sample (d). Comparison can be made here to similar results found by Canham in 1995 [15] where a microporous silicon layer on bulk Si immersed in SBF was analysed and found to form apatite spherulites within a four week period.

It can also be noted that the apatite spherulites in sample (d) are considerably larger (up to 10 microns) in size compared to the HA observed in sample (c). This is attributed to the much larger average

particle size of sample (d) of 20 microns compared to 4-6 microns for sample (c). Sample (b) showed no evidence of apatite growth after 30 days in SBF. Previous work by Canham [15] has indicated that bulk Si is considered bioinert. Sample (b) in this study was partially etched and therefore had a lower pore volume and the lowest surface area of all the silicon samples indicating that the pore depth was shallower than the other samples analysed here. It is likely that this reduced porosity level inhibited the growth of an apatite layer when compared with the other samples studied. High surface area porosity of PS has previously been deemed an essential factor necessary for establishing HA layers and subsequent bioactivity with pore size and pore volume directly related to the rate of apatite nucleation on materials [23]. The elemental concentration of surface oxygen is slightly lower in sample (b) compared to the other samples which may have also influenced its behaviour in SBF [2]. The EDX analysis (see supplementary information) of the surface layers indicated the presence of calcium and phosphorous - the principle components of HA. The EDX point spectrum obtained for Fig. 6 is highlighted in Table 3 below showing the Ca/P ratios for the selected points. Quantitative EDX (SEM) analysis (see Table 4) suggests that the Ca/P ratios for the observed calcium phosphate layers are quite similar to that of bone apatite (Ca: P of 1.67) [2, 24]. The area also showed regions of needle shaped crystals attributed to HA (see Figure. 7). With the exception of sample (b), all samples had Ca/P ratios similar to that of bone apatite (see Table 4) and needle shaped crystals attributed to HA were also observed.

Table 3 EDX normal wt % point spectrum for sample (a)

Spectrum	**Si**	**P**	**Ca**	**Total**	**Ca/P Ratio**
Spectrum 1	3.66	34.66	61.67	100	1.77
Spectrum 2	5.79	35.71	58.5	100	1.63
Spectrum 3	0.83	37.14	62.03	100	1.67

Table 4 EDX point spectrum for samples (a)-(d)

Normal wt%	Sample (a)	Sample (b)	Sample (c)	Sample (d)
Ca	62.03	0.0	62.03	62.40
P	37.14	0.0	37.7	37.58
Ca/P	1.67	N/A	1.65	1.67

3.3 TEM Analysis after SBF

TEM analysis indicated the presence of PS particles covered by a dense surface layer of large particle-like aggregates of needle shaped crystals, typified by the image in Fig. 7a. Nano-beam diffraction analysis indicated a crystalline structure as shown by Fig. 7b. The crystal structure has been matched to HA in the JPDS database (reference number 01-1008). The simulated diffraction pattern is indicated in Fig. 7b. The results shown were found to be representative of the sample as a whole, after a number of different areas were studied. The compositional elements of the surface layer, as identified by EDX indicate the presence of calcium (Ca), phosphorus (P) and silicon (Si) within the crystalline structure

(see Fig. 7c). The lower region on the left of the image in Fig. 7a shows the PS area covered by the dense crystalline apatite layer. The line across this selected area represents the TEM Line EDX spectra in Fig. 7c. The high (Si) peak shows the initial PS region which is then covered by the apatite layer and represented by high (Ca) and (P) peaks.

In Vitro SBF experiments are currently the most convenient and accurate method to test for the possible bioactivity and the bone bonding ability of a material [4, 25]. It is not always as accurate as animal trial experiments and great care must be taken to prepare the SBF solution and conduct a precise *in vitro* experiment [26]. However, short of conducting costly animal trial experiments SBF is currently the most accurate pre-animal trial test available. It allows us to reduce the number of samples tested in live animals, reducing both cost and morbidity. While there is growing interest in developing biomaterials which have more chemically reactive surfaces and elicit a desired physiological response [27], an essential requirement for tissue-bonding materials is that they can induce precipitation of a non-stoichiometric form of HA on their surfaces *in vivo. In vitro* bioactivity testing can also be used to assess the ability of various materials to produce this mineral phase of bone and has been shown to directly correlate to results *in vivo* [4, 27]. Therefore, the principal finding is that the nanoporous silicon particles used in this study are capable of forming a calcium phosphate layer at their surface which implies that a direct bond with bone tissue would be possible *in vivo*. The bioactivity of these particles may be further improved by oxidising the PS samples before SBF immersion or by coating or implanting hydrogen into the silicon particle surface and examining after exposure to SBF [28]. These experiments and exploration of the interfacial layer between the HA and silicon particle surface is part of further work to be pursued and will be promulgated in due course.

4.0 Conclusions

Using standard *in vitro* testing metallurgical grade porous silicon samples were submerged into simulated body fluid for a trial period of 30 days to determine their biocompatibility. Electron microscopy analysis clearly revealed the formation of calcium phosphate layers on fully etched samples with relatively high surface areas as determined from BET studies. Nano-beam diffraction analysis concluded that the calcium phosphate layers were crystalline HA. The formation of the apatite was found to be dependant on the level of porosity where one sample with shallower pores did not exhibit apatite growth. These results give a strong indication that metallurgical grade nanoporous silicon can be deemed bioactive and has the potential to bond directly to living bone tissue upon implantation.

Acknowledgements

The Authors would like to acknowledge the financial support of Enterprise Ireland, Vesta Sciences (EI IP 2007 0380 Vesta/ UL) and PRTLI cycle 4. EC would also like to thank Paula Olsthoorn, Gaye Hanrahan, Dr. Calum Dickinson, Dr. Anthony Wren, Dr. Tofail Syed, Dr. Fathima Laffir and Professor Shohei Nakahara for analytical results and useful discussion.

References:

1. Black J (1999) Biological Performance of Materials-Fundamentals of Biocompatibility. Marcel Dekker, America
2. Pastor E, Matveeva E, Parkhutik V, Curiel-Esparza J, Millan M.C (2007) Influence of porous silicon oxidation on its behaviour in simulated body fluid. Phys.Stat.Sol. C 4:2136-2140
3. Yao X, Yao H, Li G, Li Y (2010) Biomimetic synthesis of needle-like nano-hydroxyapatite templated by double-hydrophilic block copolymer. Journal of Materials Science 45:1930-1936
4. Kokubo T, Takadama H (2006) How useful is SBF in predicting in vivo bone bioactivity. Biomaterials 27:2907-2915
5. Pramatarova L, Pecheva E, Dimova-Malinovska D, Pramatarova R, Bismayer U, Petrov T, Minkovski N (2004) Porous silicon as a substrate for hydroxyapatite growth. Vacuum 76:135-138
6. Heo K, Yoon J, Jin K.S, Jin S, Ree M (2006) Characterisation of pore structures in nanoporous materials for advanced bionanotechnology. IEE Pro-Nanobiotechnology 153:121-128
7. Reddy R.R.K, Chadha A, Bhattacharya E (2001) Porous silicon based potentiometric triglyceride biosensor. Biosensors and Bioelectronics 16:313-317
8. Niu Y, Liu X, Ding C (2008) Vacuum-plasma-sprayed silicon coatings for biomedical application. Materials Science & Engineering C 28:1132-1137
9. Presting H, Konle J, Starkov V, Vyatkin A, Konig U (2004) Porous silicon for micro-sized fuel cell reformer units. Materials Science and Engineering B 108:162-165
10. Subramanian S, Tiegs T, Limaye S (2008) Nanoporous Silicon Based Energetic Materials. 26th Army Science Conference-Nanotechnology
11. Anglin E, Cheng L, Freeman W, Sailor M (2008) Porous silicon in drug delivery devices and materials. Advanced Drug Delivery Reviews 60: 1266-1277
12. Shaoqiang C, Ziqiang Z, Jianzhong Z, Jian Z, Yanling S, Ke Y, Weiming Wang, Xiaohua W, Xiao F, Laiqiang L, Li S (2004) Hydroxyapatite coating on porous silicon substrate obtained by precipitation process. Applied Surface Science 230:418-424
13. Canham L (2000) Porous silicon as a therapeutic biomaterial. Microtechnologies in Medicine and Biology, 1st Annual International IEEE Conference 109-112
14. Jarvis K, Barnes T.J, Prestidge, C.A, Badalyan A, Pendleton P (2006) Porous Silicon - A Nanostructured Delivery System. International Conference on Nanoscience and Nanotechnology 536-539
15. Canham L.T (1995) Bioactive Silicon Structure Fabrication Through Nanoetching Techniques. Advanced Materials 7:1033-1037
16. Low S.P, Williams K.A, Canham L.T, Voelcker N.H (2009) Generation of reactive oxygen species from porous silicon microparticles in cell culture medium. Journal of Biomedical Materials Research Part A 3:1124-1131
17. Farrell D, Limaye S, Sybramanian S (2006) Silicon Nanosponge Particles. World Intellectual Property Organisation-Patent WO2006/121870A2
18. British Standards ISO (2007) Implants for surgery - In vitro evaluation for apatite-forming ability of implant materials. BS ISO-Patent 23317:2007
19. Brunauer S, Emmett P.H, Teller Edward (1938) Adsorption of Gases in Multimolecular Layers. Journal of the American Chemical Society 60:309-319
20. Barrett E.P, Joyner L.G, Halenda P.P (1951) The Determination of Pore Volume and Area Distributions in Porous Substances. I. Computations from Nitrogen Isotherms. Journal of the American Chemical Society 73:373-380
21. Wren A, Boyd D, Towler M.R (2008) The processing, mechanical properties and bioactivity of strontium based glass polyalkenoate cements. Journal of Materials Science: Materials in Medicine 19:1737-1743
22. Lee J, Cho S, Lee S, Rhee S (2009) Nucleation and growth mechanism of apatite on a bioactive and degradable ceramic/polymer composite with a thick polymer layer. Journal of Materials Science 44:4531-4538
23. Horcajada P, Ramila A, Boulahya K, Gonzalez-Calbet J, Vallet-Regi M (2004) Bioactivity in ordered mesoporous materials. Solid State Sciences 6: 1295-1300
24. Dorozhkin S (2009) Calcium orthophosphate-based biocomposites and hybrid biomaterials. Journal of Material Science 44: 2343-2387

25. Coffer J.L, Whitehead M.A, Nagesha D.K, Mukherjee P, Akkaraju G, Totolici M, Saffie R.S, Canham L.T (2005) Porous silicon-based scaffolds for tissue engineering and other biomedical applications. Physica status solidi (a) 202:1451-1455
26. Bohner M, Lemaitre J (2009) Can bioactivity be tested in vitro with SBF solution. Biomaterials 30:2175-2179
27. Canham L.T, Reeves C.L, Loni A, Houlton M.R, Newey J.P, Simons A.J, Cox T.I (1997) Calcium phosphate nucleation on porous silicon: factors influencing kinetics in acellular simulated body fluids. Thin solid films 297:304 -307
28. Liu X, Fu R, Poon R, Chen P, Chu P, Ding C (2004) Biomimetic growth of apatite on hydrogen-implanted silicon. Biomaterials 25:5575-5581

FIGURE CAPTIONS

Fig. 1. (a) An SEM image for PS sample (a) indicating the surface morphology. Inset image shows the dispersion of pores. (b) A TEM image for sample (a) showing the surface morphology. The inset image shows the porosity at the outer region of the Si particle.

Fig. 2. SEM images of the PS samples (a)-(d) before immersion into SBF.

Fig. 3. SEM-EDX analysis of the PS samples (a) and (b) before immersion into SBF

Fig. 4. XPS spectrum analysis of the PS samples (a) and (b) before immersion into SBF

Fig. 5. SEM images of the PS samples (a)-(d) after immersion into SBF

Fig. 6. SEM image of the PS sample (a) after immersion into SBF

Fig. 7. (a) Bright Field TEM micrograph of surface apatite layer of sample (a) after 30 day immersion in SBF (b) Nano-Beam diffraction pattern from (a) showing crystalline structure (c) Inset on the top left shows the Line-EDX analysis starting from left to right as indicated by the line at the bottom of the image (The PS region is on the left of the line while the needle-like apatite structure is on right)

Fig. 1. (a) An SEM image for PS sample (a) indicating the surface morphology. Inset image shows the dispersion of pores. (b) A TEM image for sample (a) showing the surface morphology. The inset image shows the porosity at the outer region of the Si particle.

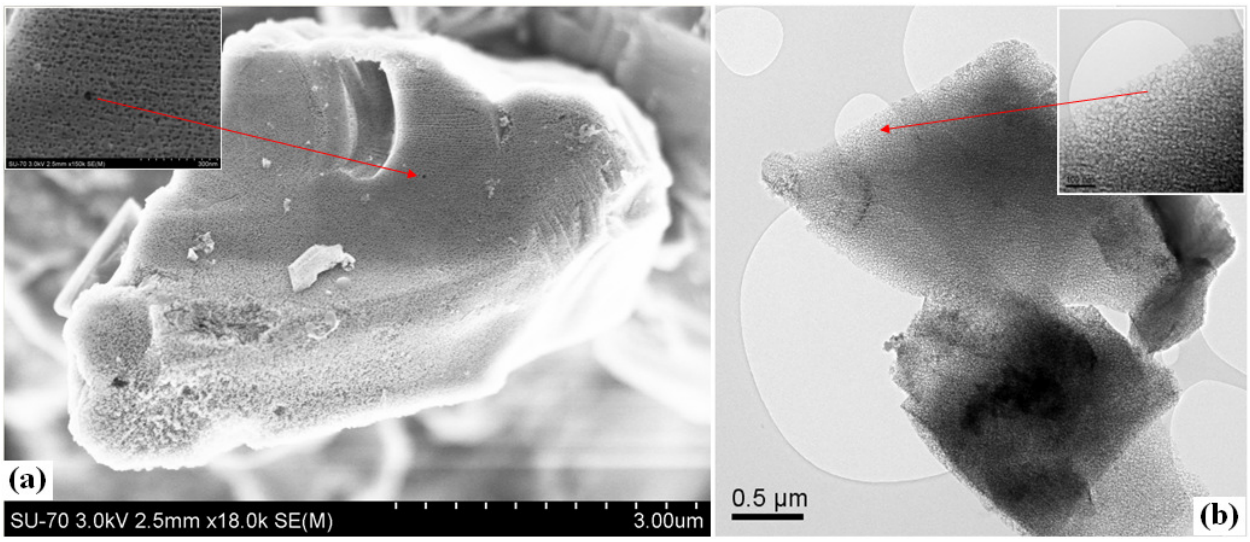

Fig. 2. SEM images of the PS samples (a)-(d) before immersion into SBF.

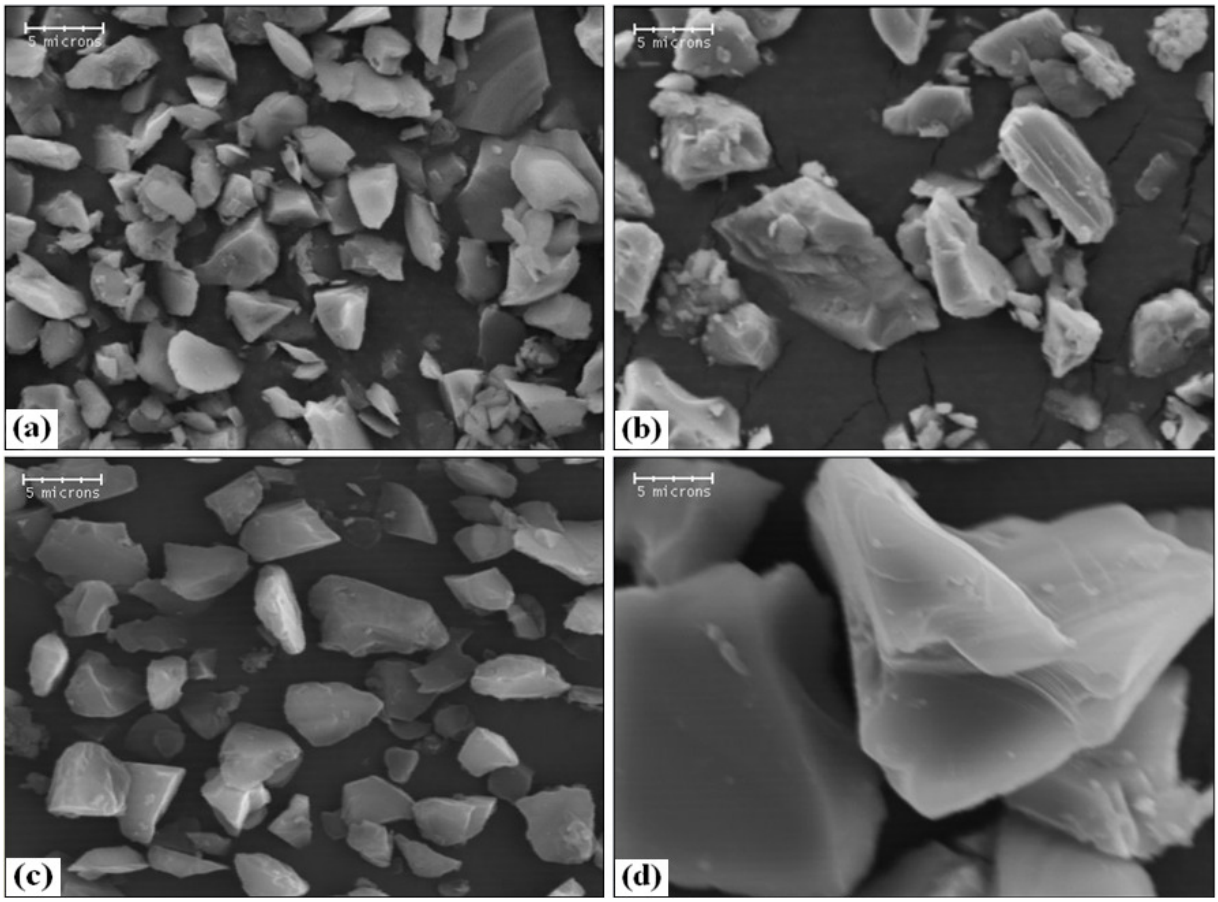

Fig. 3. SEM-EDX analysis of the PS samples (a) and (b) before immersion into SBF

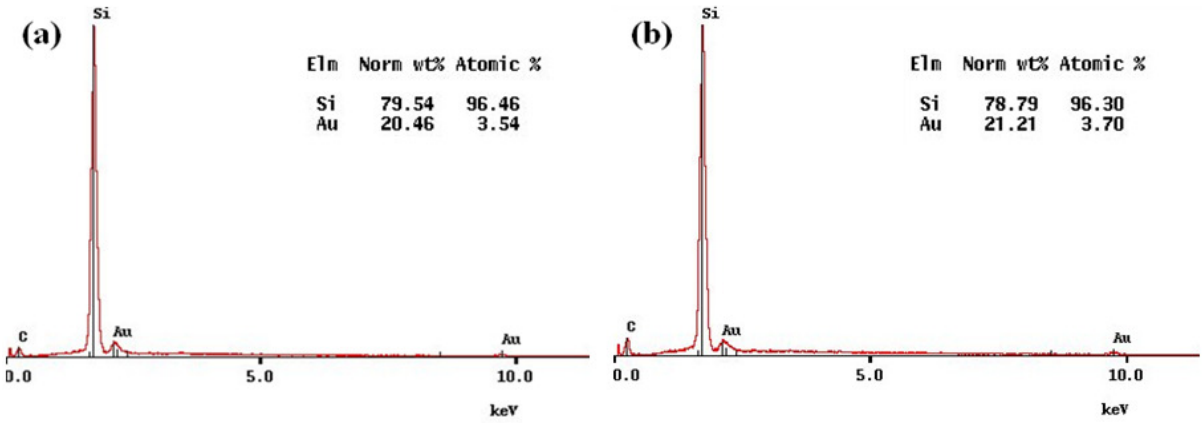

Fig. 4. XPS spectrum analysis of the PS samples (a) and (b) before immersion into SBF

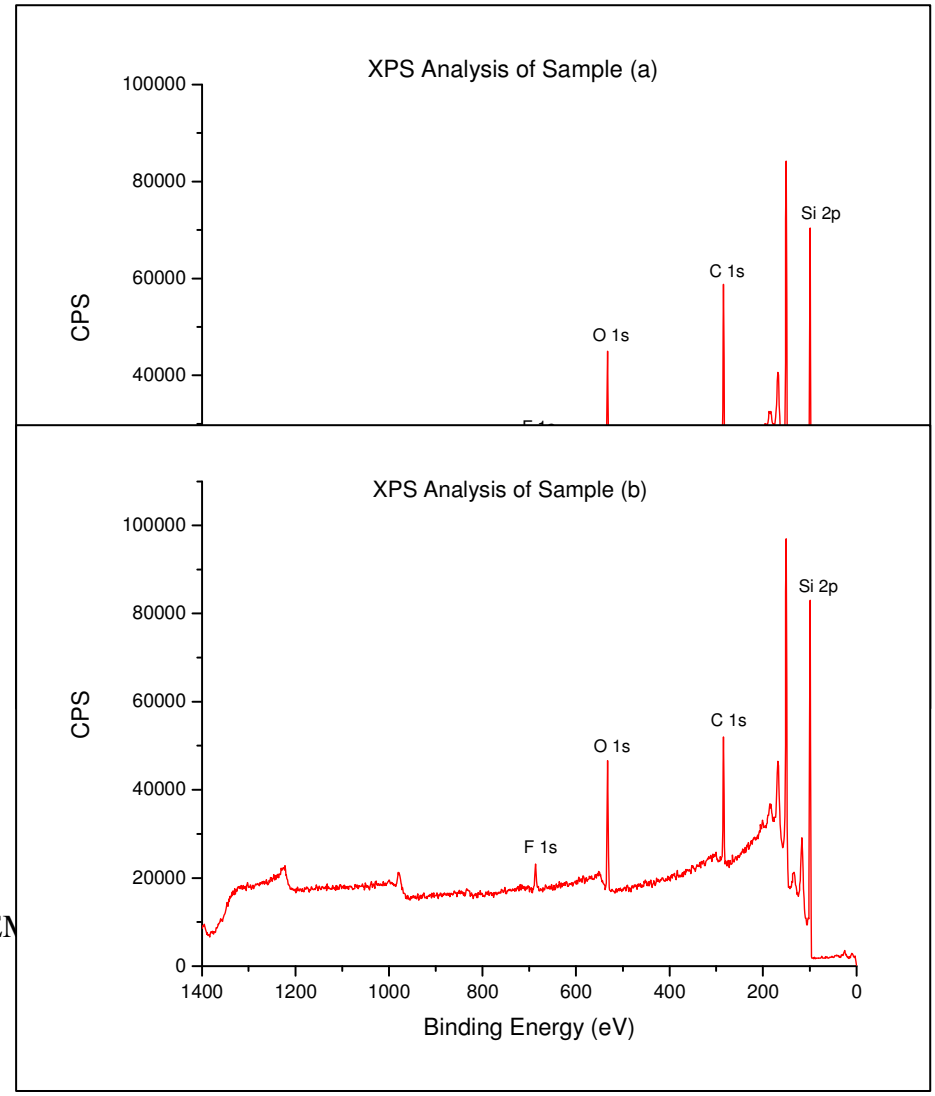

Fig. 5. SEM

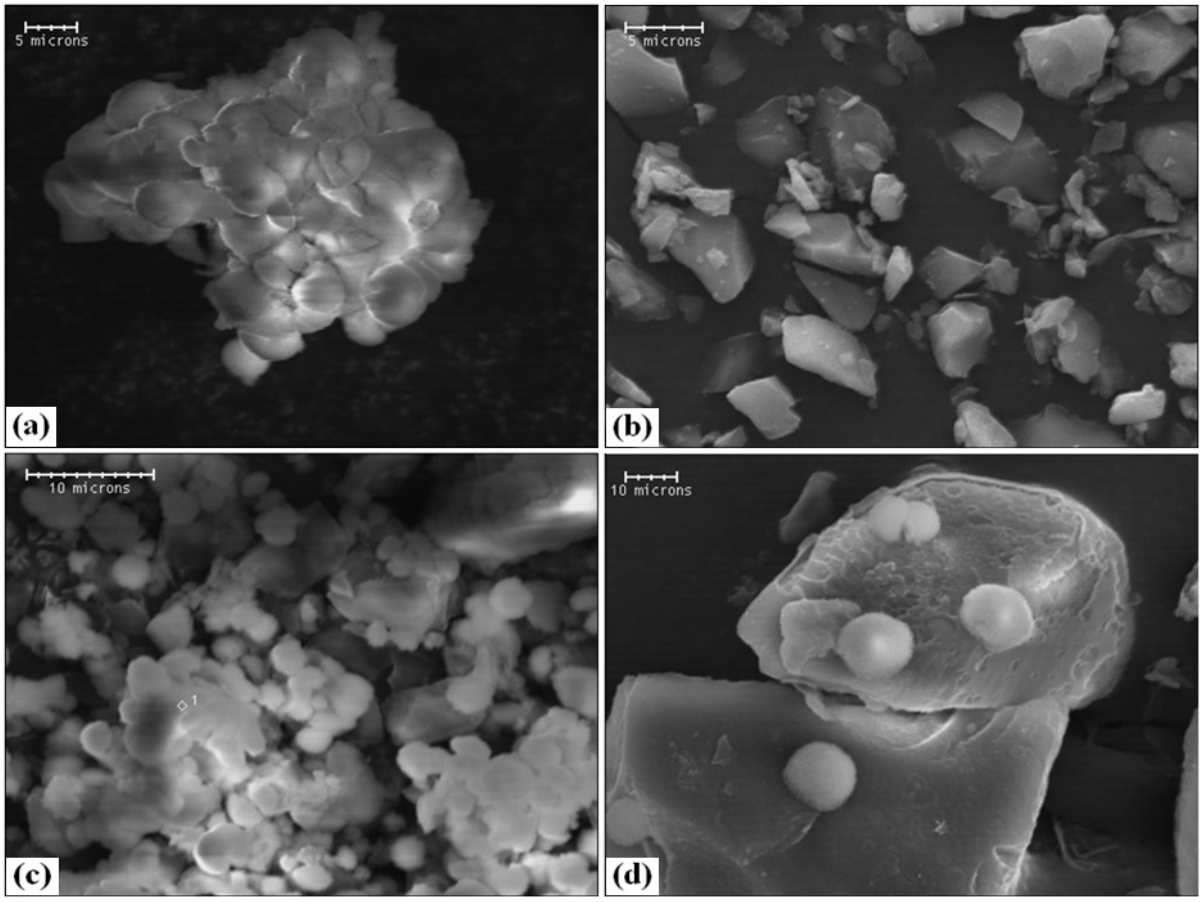

Fig.6. SEM image of the PS sample (a) after immersion into SBF

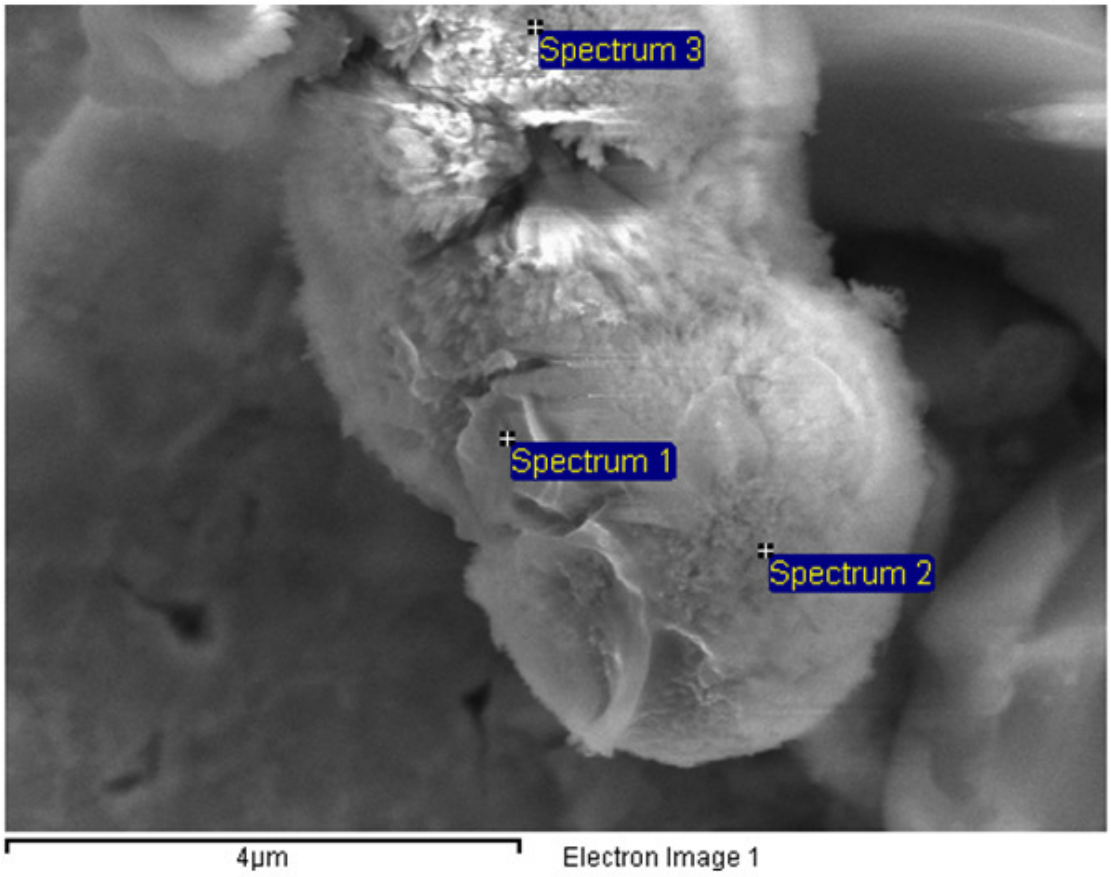

Fig. 7. (a) Bright Field TEM micrograph of surface apatite layer of sample (a) after 30 day immersion in SBF (b) Nano-Beam diffraction pattern from (a) showing crystalline structure (c) Inset on the top left shows the Line-EDX analysis starting from left to right as indicated by the line at the bottom of the image (The PS region is on the left of the line while the needle-like apatite structure is on right)

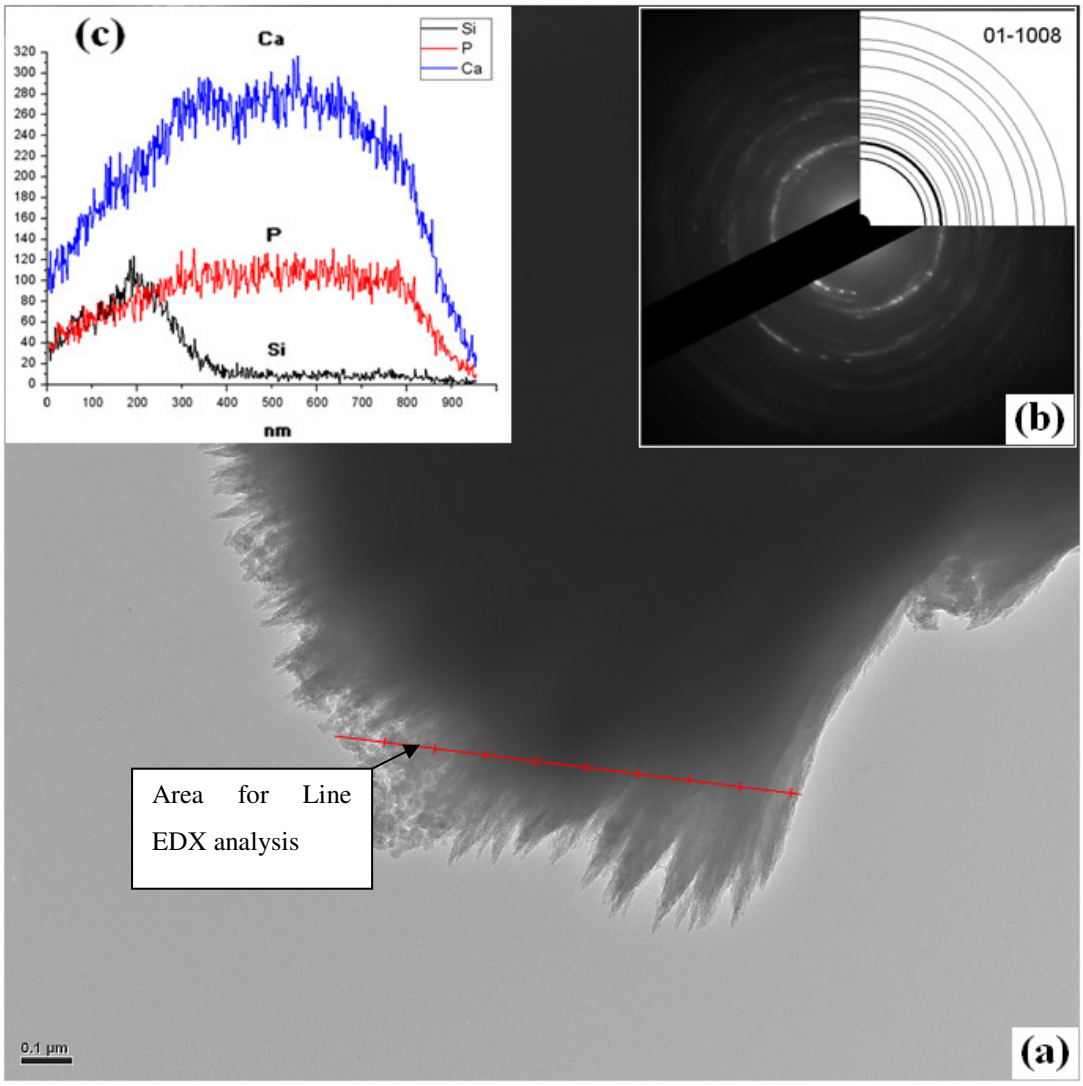
(c)
Ca
P
Si
Si
P
Ca
nm
01-1008
(b)
Area for Line EDX analysis
0.1 µm
(a)

APPENDIX A

1. SEM EDX of the PS samples (a)-(d) after immersion into SBF